Available online at www.sciencedirect.com
SCIENCE DIRECT®
Journal of Solid State Chemistry 178 (2005) 3686–3697
JOURNAL OF SOLID STATE CHEMISTRY
www.elsevier.com/locate/jssc

Synthesis and structural, spectroscopic and magnetic studies of two new polymorphs of $Mn(SeO_3) \cdot H_2O$

Aitor Larrañaga[a], José L. Mesa[b,*], José L. Pizarro[a], A. Peña[b], Roger Olazcuaga[c], María I. Arriortua[a], Teófilo Rojo[b,*]

[a]*Departamento de Mineralogía y Petrología, Facultad de Ciencia y Tecnología, Universidad del País Vasco, Apdo. 644, E-48080 Bilbao, Spain*
[b]*Departamento de Química Inorgánica, Facultad de Ciencia y Tecnología, Universidad del País Vasco, Apdo. 644, E-48080 Bilbao, Spain*
[c]*ICMCB-CNRS[UPR9048], Bordeaux 1, 87 Av. A. Schweitzer, 33608 Pessac Cedex, France*

Received 4 July 2005; received in revised form 14 September 2005; accepted 15 September 2005
Available online 25 October 2005

Abstract

Two new manganese(II) selenite polymorphs with formula $Mn(SeO_3) \cdot H_2O$ have been synthesized by slow evaporation from an aqueous solution. The crystal structure of both compounds **(1)** and **(2)** have been solved from X-ray diffraction data. The structure of **(1)** was determined from single-crystal X-ray diffraction techniques. The compound crystallizes in the *Ama*2 space group, with $a = 5.817(1)$, $b = 13.449(3)$, $c = 4.8765(9)$ Å and $Z = 4$. The structure of **(2)** has been solved from X-ray powder diffraction data. This phase crystallizes in the $P2_1/n$ space group with unit-cell parameters of $a = 4.921(3)$, $b = 13.121(7)$, $c = 5.816(1)$ Å, $\beta = 90.03(2)^\circ$ and $Z = 4$. Both polymorphs exhibit a layered structure formed by isolated sheets of MnO_6 octahedra and $(SeO_3)^{2-}$ trigonal pyramids in the (010) plane. These layers, which contain one manganese and selenium atom crystallographically independent, are formed by octahedra linked between them through the selenite oxoanions. The difference of both compounds consists in the stacking of the layers along the *b*-axis. The IR spectra show the characteristic bands of the selenite anion. Studies of luminescence performed at 6 K and diffuse reflectance spectroscopy have been carried out for both phases. The *Dq* and Racah (*B* and *C*) parameters, from luminescence and diffuse reflectance spectroscopy, are $Dq = 705$, $B = 750$, $C = 3325\,cm^{-1}$ for **(1)** and $Dq = 720$, $B = 745$, $C = 3350\,cm^{-1}$ for **(2)**. The ESR spectra of both compounds are isotropic with *g*-values of 1.99(1). Magnetic measurements indicate the presence of antiferromagnetic couplings in both phases. The *J*-exchange parameters have been estimated by fitting the experimental magnetic data to a model for square-planar lattice. The values obtained are $J/k = -0.83$, -0.91 K and $J'/k = -0.97$, -1.20 K, for polymorphs **(1)** and **(2)**, respectively.

Keywords: X-ray diffraction; Single-crystal and powder; IR; Visible–UV; Luminiscence; ESR; Magnetic susceptibility

1. Introduction

An important area in materials science is the design of compounds with an open framework, which can give rise to original physical properties with potential practical applications such as ion exchange, surface absorption chemistry, etc., due to the diversity of available cations and the arrangements that they can exhibit [1,2]. In this way, the crystal chemistry of selenium(IV) compounds shows abundant structural versatility expressed by the significant number of different compounds [3]. The transition metal–selenium–oxygen system has been the subject of many previous investigations. Several phases have been reported in which selenium is found in an oxidation state IV. Depending on the conditions in solution [4], transition metal compounds with $(HSeO_3)^-$, $(SeO_3)^{2-}$ or $(Se_2O_5)^{2-}$ oxoanions are known [5–7]. Ions with an sp^3 hybrid lone pair, such as, Se^{4+} play a peculiar role in crystal chemistry because of their high polarizability and strong preference for unusual stereochemistry [3,8]. Thus, it can be predicted that the combination of asymmetric $(SeO_3)^{2-}$ group with various transition metals will result in a rich structural chemistry in transition metal selenites. In this way, in the $Mn_4(H_2O)_3(SeO_4)_3$ and $Mn_3(H_2O)(SeO_3)$ phases [9] which

*Corresponding authors. Fax: +34 946013500.
E-mail addresses: qipmeruj@lg.ehu.es (J.L. Mesa), qiproapt@lg.ehu.es (T. Rojo).

0022-4596/$ - see front matter © 2005 Elsevier Inc. All rights reserved.
doi:10.1016/j.jssc.2005.09.034

exhibit a three-dimensional crystal structure constructed by chains, there exist cavities delimited by the MnO_6 octahedra and SeO_3 trigonal pyramids, with the lone pair, in an sp^3 hybrid orbital, pointing towards the center of cavities. Similarly, the two $Mn(SeO_3)$ polymorphs [10] also exhibit a three-dimensional crystal structure formed by chains that give rise to hexagonal channels with the lone electronic pair directed towards the center of these channels.

The crystal structures of the above-indicated three-dimensional phases are more compact than the layered crystal structures of the title compounds, probably due to the different synthetic conditions. $Mn_4(H_2O)_3(SeO_4)_3$ and $Mn_3(H_2O)(SeO_3)$ [9] were prepared by mild hydrothermal synthesis at, approximately, 170 °C and 10 atm., the two polymorphs of $Mn(SeO_3)$ [10] were obtained using supercritical hydrothermal conditions (500 or 600 °C and 500 or 1100 atm., for every polymorph), whereas the two polymorphs of $Mn(SeO_3)\cdot H_2O$ were synthesized at room temperature and pressure by slow evaporation from an aqueous solution.

Recently, Harrison et al. [11] and Choudhury et al. [12] have prepared organically templated zinc and iron selenites by using mild hydrothermal conditions. Later, Udayakumar and Rao [13] were able to synthesize, using the piperazinium cation as structure directing agent, a family of organically templated compounds in which both the hydrogenselenite and diselenite oxoanions exist simultaneously in the inorganic skeleton. On the other hand, hydrothermal synthesis performed at moderate or high temperature and pressure can be used to obtain new condensed selenites [9,10]. The synthetic procedure carried out at room temperature and pressure is also an adequate method to obtain purely inorganic compounds with low structural dimensionality. In this work we report the synthesis in aqueous solution at room temperature, the crystal structure and the thermal, spectroscopic and magnetic properties of two new layered polymorphs in the system Mn(II)–$(SeO_3)^{2-}$ with formula $Mn(SeO_3)\cdot H_2O$.

2. Experimental

2.1. Synthesis and characterization

The new polymorphs of $Mn(SeO_3)\cdot H_2O$, compounds **(1)** and **(2)**, have been synthesized by slow evaporation from an aqueous solution containing $MnCl_2\cdot 4H_2O$ (5.05 mmol) and SeO_2 (9.0 mmol). The pH of the reaction mixtures was increased to, approximately, 7 using RbOH and 6.5 using NH_4OH for compounds **(1)** and **(2)**, respectively. After 2 days at room temperature, the evaporation of water yielded light-pink single crystals in the case of phase **(1)** and a microcrystalline powder for compound **(2)** of the same color. The resulting products were filtered, washed with water and acetone and dried over P_2O_5 for 6 h.

The percentage of the elements in the products was determined by inductively coupled atomic emission spectroscopy (ICP-AES). Observed (%): Mn, 27.2 and 27.3; Se, 39.3 and 39.2. $Mn(SeO_3)\cdot H_2O$ **(1)** and **(2)**. Calculated: (%) Mn, 27.5; Se, 39.5. The density, measured by picnometry in kerosene, was 3.5(1) g cm^{-3} for both phases.

Thermogravimetric analysis was carried out under an oxygen atmosphere in a SDC 2960 Simultaneous DSC-TGA TA Instrument, at 5 °C min^{-1} in the temperature range 30–800 °C. A crucible containing ca. 20 mg of sample was used. The decomposition curves for both phases reveal two different steps. The first, in the 125–300 and 200–295 °C ranges for **(1)** and **(2)**, respectively, corresponds to the elimination of water. The experimental loss is approximately, 11% and 9%, for **(1)** and **(2)**, respectively, the calculated loss being 9%. The second step corresponds to the decomposition of the $(SeO_3)^{2-}$ anion in the form of SeO_2 gas, and takes place in the 450–550 and 460–560 °C ranges, for compounds **(1)** and **(2)**. The loss experimental is 51.2%, 51.4%, for **(1)** and **(2)**, respectively, the calculated loss being 51.5%. The X-ray powder diffraction patterns of the residues obtained at 800 °C show the presence of Mn_2O_3 [space group $Ia3$, $a = 9.43(1)$ Å] [14].

The thermal behavior of these polymorphs was also studied by time-resolved X-ray thermodiffractometry. The X-ray powder patterns were collected in air on a PHILIPS X'PERT automatic difractometer (Cu-$K\alpha$ radiation) equipped with a variable-temperature stage (Paar Physica TCU2000) with a Pt sample holder. The patterns were recorded in 2θ steps of 0.02° in the range 5–40°, counting for 2 s per step and increasing the temperature at 5 °C min^{-1} from room temperature up to 800 °C. The results are given in Figs. 1a and b. Polymorph **(1)** is stable up to approximately 225 °C. A strong decrease of the peak intensities is observed in the 225–350 °C range, indicating the decomposition of the compound to give an amorphous phase. At temperatures higher than 350 °C a crystalline intermediate phase is formed, which cannot be identified in the Powder Diffraction File. Finally, at temperatures higher than 415 °C the inorganic residue is the Mn_2O_3 oxide [14], which is in good agreement with that obtained from the thermogravimetric study (see Fig. 1a). Polymorph **(2)** is stable up to approximately 250 °C. In the 250–475 °C range the same crystalline intermediate compound is formed. In the case of compound **(1)**, the residue obtained at 800 °C is Mn_2O_3, in accordance with the thermogravimetric analysis (see Fig. 1b).

2.2. Crystal structure determination of the polymorphs *(1)* and *(2)*

2.2.1. Polymorph (1)

A prismatic single crystal of **(1)** with dimensions $0.02\times0.02\times0.01$ mm^3 was carefully selected under a polarizing microscope. This crystal was used for the data collection performed on an XCALIBUR2 automated diffractometer equipped with a CCD detector, using graphite-monochromated Mo-$K\alpha$ radiation. The total number of measured reflections was 1653, with 479

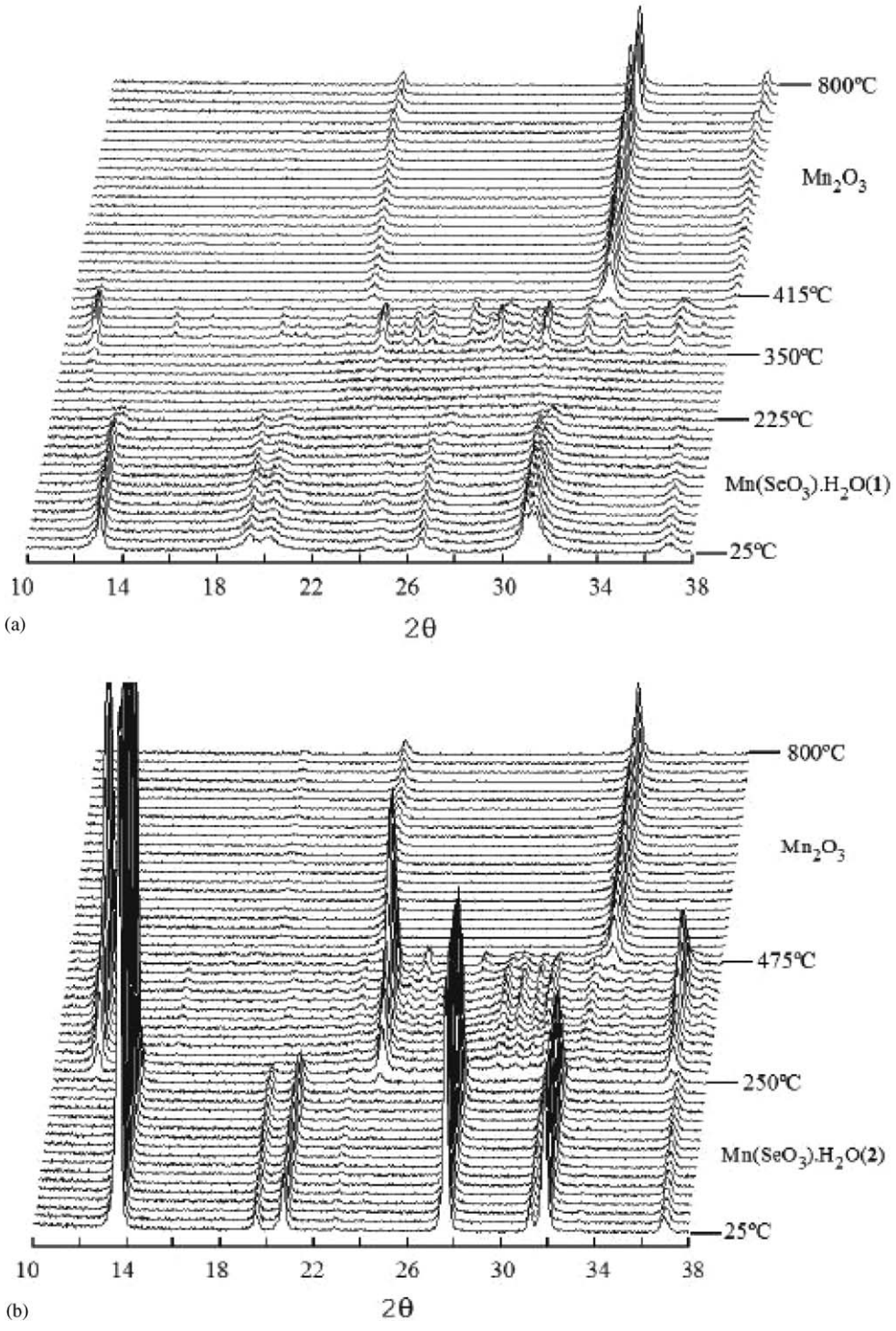

Fig. 1. Thermodifractograms of (a) polymorph **(1)** and (b) polymorph **(2)**.

reflections being independent ($R_{int.} = 0.1046$) and 476 observed, applying the criterion $I > 2\sigma(I)$. The Lorentz polarization and absorption corrections were made with the diffractometer software [15], taking into account the shape and size of the single crystal. The structure was solved by direct methods with the program SHELXS97 [16] belonging to the WINGX system [17]. The manganese and selenium atoms were located directly and the oxygen atoms from Fourier difference maps. The hydrogen atoms of the water molecule were not determined. The refinement procedure of the crystal structure was carried out by the full-matrix least-squares method based on F^2, using the SHELXL97 computer program [18]. A restraint was imposed in the refinement, due to the absence of inversion

Table 1
Crystal data, intensity collection and some features of the structure refinement for **(1)** from single crystal data

Empirical formula	$MnSeO_3 \cdot H_2O$
Formula weight (g/mol)	199.91
Temperature (K)	293(2)
Wavelength (Å)	0.71073
Crystal system, space group	Orthorhombic, *Ama*2
a (Å)	5.817(1)
b (Å)	13.449(3)
c (Å)	4.8765(9)
Volume (Å^3)	381.5(1)
Z, calculated density (g/cm^3)	4, 3.445
Absorption coefficient (mm^{-1})	12.854
F(000)	364
Crystal size (mm^3)	$0.02 \times 0.02 \times 0.01$
Diffractometer	Xcalibur2
θ range for data collection (deg.)	4.45–31.69
Limiting indices	$-8<h<8$, $-19<k<19$, $-7<l<4$
Reflections collected/unique	1653/479 [R(int) = 0.1046]
Completeness to θ (%)	96.1
Refinement method	Full-matrix least-squares on F^2
Data/restraints/parameters	476/1/34
Goodness-of-fit on F^2	1.299
Final R indices [$I>2\sigma(I)$]	$R_1 = 0.0679$, w$R_2 = 0.1648$
R indices (all data)	$R_1 = 0.0682$, w$R_2 = 0.1649$
Largest diff. peak and hole (e Å^{-3})	1.402 and −1.329

$R_1 = [\Sigma(|F_o| - |F_c|)]/\Sigma|F_o|$; $wR_2 = [\Sigma[w(|F_o|^2 - |F_c|^2)^2]/\Sigma[w(|F_o|^2)^2]]^{1/2}$; $w = 1/[\sigma^2|F_o|^2 + (xp)^2 + (yp)]$; where $p = [|F_o|^2 + 2|F_c|^2]/3$; $x = 0.0644$, $y = 9.1281$.

center in the spatial group *Ama*2. The scattering factors were taken from Ref. [19]. All atoms were refined anisotropicaly reaching final R factors of $R_1 = 0.0682$ [w$R_2 = 0.1649$] (all data). Maximum and minimum peaks in final difference map were 1.402, −1.329 e Å^{-3}. Details of the crystal data, intensity collection and some features of the structural refinement are reported in Table 1. The structure parameters have been deposited at the FIZ-Karlsruhe Centre (CSD 415549).

2.2.2. Polymorph (2)

Although polymorph **(2)** is isotypic with Co$(SeO_3) \cdot 2H_2O$ [20], attempts to resolve the crystal structure starting from that of the cobalt(II) phase, did not yield good reliability R-factors, due to the structural differences in the stacking of the layers in the Mn(II) and Co(II) isotypic phases.

The exact positions of the first 20 maxima of the diagram of **(2)** were obtained with the WINPLOTR program [21]. The indexation of these peaks was carried out with the TREOR90 program [22], giving as the best cell, $a = 5.81(1)$, $b = 13.11(1)$, $c = 4.91(1)$ Å and $\alpha \approx \beta \approx \gamma \approx 90^\circ$. This unit cell is close to that of the orthorhombic polymorph **(1)**. The pattern matching refinement performed with an orthorhombic symmetry did not allow a good fit of the diffractogram, so, a monoclinic cell with β near 90° was used to obtain a reasonable agreement between the calculated and observed data. The analysis of the systematic absences ($0k0$; $k = 2n$ and $h0l$; $h + l = 2n$) indicated that the $P2_1/n$ is the more probable space group.

The preferred orientation (010) observed during the characterization of compound **(2)** together with the similarity of the powder diffractograms and the cell parameters of both compounds, allowed us to consider a similar layered structure for both polymorphs.

Taking into account geometric features, structural models that fulfill the three following conditions were considered: (i) the compound has (010) layers, (ii) the sheets have the same topology than the layers observed in compound **(1)**, (iii) the structural model must be in accord with the $P2_1/n$ monoclinic symmetry. This process was monitored comparing the theoretical diagrams for each model using the ATOMS program [23] and the experimental X-ray diffractogram from polymorph **(2)**.

The Rietveld refinement (FULLPROF98 program) [24] obtained using the best structural model gives rise to a good agreement between the observed and calculated diffractograms. Soft constrains for the Se–O and Mn–O distances were used in the last refinement taking into account the (010) preferred orientation (Fig. 2a). Fig. 2b shows the comparison of a region of the powder patterns for polymorphs **(1)** and **(2)**. Additional maxima are observed in **(1)** or **(2)** near to $2\theta \approx 23^\circ$, due to its different symmetry.

The final structural parameters and R-factors are shown in Table 2. Atomic coordinates of both compounds are given in Table 3. The structure parameters have been deposited at the FIZ-Karlsruhe Centre (CSD 415550).

2.3. Physicochemical characterization techniques

The IR spectra (KBr pellets) were obtained with a Nicolet FT-IR 740 spectrophotometer in the 400–4000 cm^{-1} range. Luminescence measurements were carried out on a Spectrofluorimeter Fluorolog-2 SPEX 1680, model F212I at 6.0 K. The excitation source was a high-pressure xenon lamp emitting between 200 and 1200 nm. Diffuse reflectance spectra were registered at room temperature on a Cary 2415 spectrometer in the 210–2000 nm range. A Bruker ESP 300 spectrometer was used to record the ESR polycrystalline spectra. The temperature was stabilized with an Oxford Instrument (ITC 4) regulator, the magnetic field was measured with a Bruker BNM 200 gaussmeter and the frequency inside the cavity was determined using a Hewlett-Packard 5352B microwave frequency counter. Magnetic measurements on powdered samples were performed in the temperature range 5–300 K, using a Quantum Design MPMS-7 SQUID magnetometer. The magnetic field was of 0.1 T, a value in the range of linear dependence of magnetization vs. magnetic field even at 5 K.

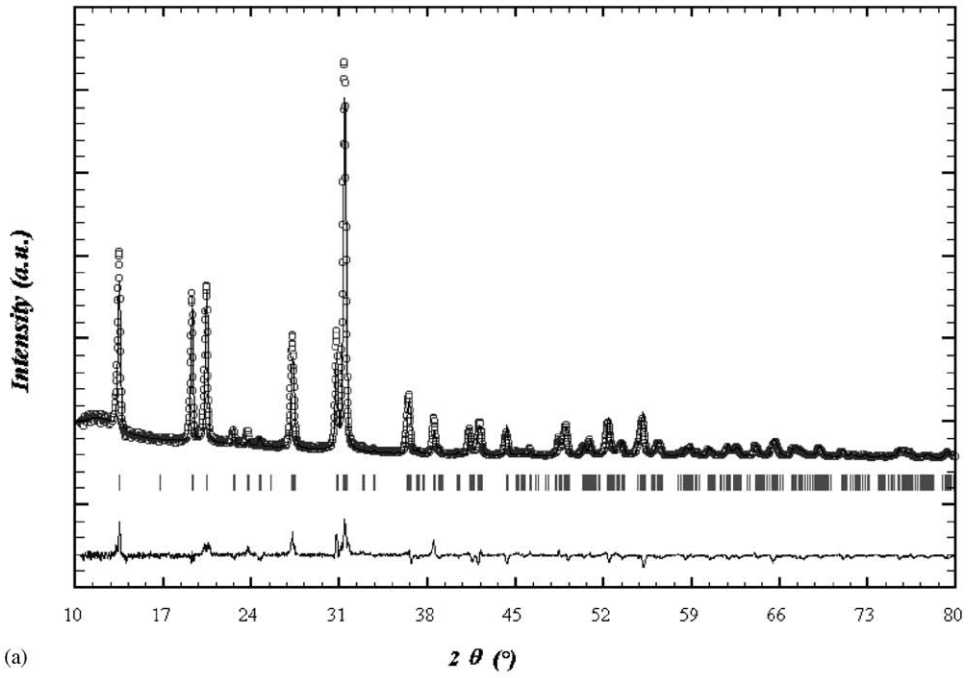

(a)

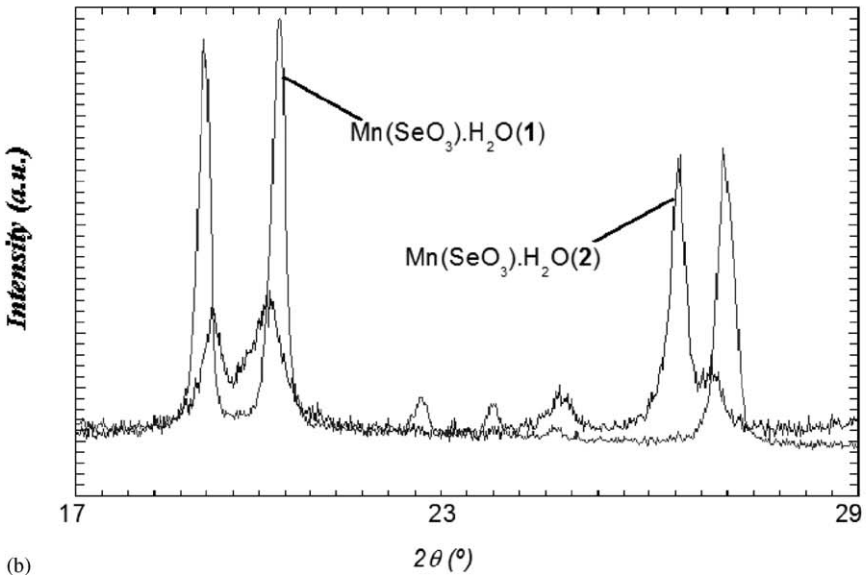

(b)

Fig. 2. (a) Observed, calculated and difference X-ray powder diffraction patterns of polymorph (**2**). The observed data are shown by dots; the calculated pattern by a solid line with the difference below. (b) A selected region of the powder patterns of polymorphs (**1**) and (**2**) showing the differences near at $2\theta \approx 23^{\circ}$.

3. Results and discussion

3.1. Structural description of polymorphs (1) and (2)

Polymorphs **(1)** and **(2)** of $Mn(SeO_3) \cdot H_2O$ exhibit a layered crystal structure constructed from (010) isolated sheets of MnO_6 octahedra and $(SeO_3)^{2-}$ trigonal pyramids. These layers, which contain one crystallografically independent manganese and selenium atom, are formed by octahedra linked through corner sharing and selenite oxoanions (Fig. 3).

It is worth mentioning that the two polymorphs show different orientation of the layers (Fig. 4). In polymorph **(1)**, two adjacent sheets are related by one "*a*" symmetry plane and the binary axes parallel to the *c*-axis, being separated by 3.37(1) Å. In polymorph **(2)**, the layers are related by twofold screw axes parallel to the *b*-axis and by inversion centers. These sheets are rotated 180° and separated by 3.28(1) Å. As consequence of these structural features compound **(1)** exhibits orthorhombic symmetry, whereas that the symmetry for phase **(2)** is monoclinic.

Table 2
Crystal data, intensity collection and some features of the structure refinement for **(2)** from powder data

Empirical formula	$MnSeO_3 \cdot H_2O$
Formula weight (g/mol)	199.91
Temperature (K)	293(2)
Wavelength (Å)	1.5406
Crystal system, space group	Monoclinic, $P2_1/n$
a (Å)	4.921(3)
b (Å)	13.121(7)
c (Å)	5.816(1)
β (deg.)	90.03(2)
Volume (Å^3)	375.5(4)
Z, calculated density (g/cm^3)	4, 3.499
Absorption coefficient (mm^{-1})	38.684
$F(000)$	364
Diffractometer	X'Pert
θ range for data collection (deg.)	10.10–79.96
2θ step-scan increment (deg.)	0.020
Time-step (s/step)	12
No. of points	3494
No. of reflections/independent	568/232
No. of structural parameters	19
No. of profile parameters	12
Scale factor	1
No. atoms refined	6
R_{Bragg}, R_f (%)	7.19, 4.95
R_p, wR_p(%)	5.34, 6.78
χ^2	2.25

$R_p = \Sigma|yi_{obs} - (1/c)yi_{calc}|/\Sigma yi_{obs}$;
w$R_p = [\Sigma_{wi}|yi_{obs} - (1/c)yi_{calc}|^2]/\Sigma wi[yi_{obs}]^2]^{1/2}$;
$R_B = \Sigma|I_{obs} - I_{calc}|/\Sigma I_{obs}$.

Table 3
Atomic coordinates and equivalent isotropic displacement parameters $U_{(eq)}$ (Å^2) for **(1)** and **(2)**

	x	y	z	$U_{(eq)}$
(1)				
Se(1)	0.7500	0.1014(1)	−0.0054(2)	0.0166(4)
Mn(1)	0.7500	0.2675(2)	0.5670(7)	0.0180(6)
O(1)	0.7500	0.138(1)	0.313(3)	0.024(3)
O(2)w	0.7500	0.388(1)	0.876(4)	0.026(3)
O(3)	0.529(2)	0.1691(8)	−0.157(2)	0.022(2)
(2)				
Se(1)	1.0253(5)	0.4026(1)	0.755(1)	0.028(8)
Mn(1)	0.1029(7)	0.2684(2)	0.248(2)	0.012(8)
O(1)w	0.416(2)	0.3908(8)	0.28(1)	0.031(19)
O(2)	0.858(3)	0.346(1)	0.982(2)	0.021(16)
O(3)	0.884(3)	0.329(1)	0.548(2)	0.014(15)
O(4)	1.348(2)	0.3661(7)	0.716(4)	0.08(2)

$U_{eq} = (\frac{1}{3})[(U_{11}(aa^*)^2 + U_{22}(bb^*)^2 + U_{33}(cc^*)^2 + 2U_{13}aca^*c^* \cos\beta]$.

The rotation of the layers in polymorph **(2)** determines that the selenite groups are in alternated disposition in adjacent sheets, with the vertex belonging to the edge not shared in opposite directions. However, in polymorph **(1)** the oxygen atoms from the edge not shared follow the same direction (see Fig. 3). The application of the symmetry elements of every space group generates a displacement of the layers along the [100] direction for polymorph **(2)**. This structural feature is not observed for polymorph **(1)** (see Fig. 4).

In polymorph **(1)** the MnO_6 octahedra are linked to four $(SeO_3)^{2-}$ anions through four O(3) and one O(1) oxygen atoms, the six-fold coordination is completed by the O(2) from the water molecule. In polymorph **(2)** the hexacoordination of the Mn(II) cations is achieved by the two O(4), two O(2) and one O(3) belonging to the selenite groups and one O(1) from the water molecule (Fig. 5). In polymorph **(1)** the links between the MnO_6 octahedra is via four O(3). For polymorph **(2)** the links between the MnO_6 groups is achieved by two O(2) and two O(4) common vertices between the octahedra and the selenite anions (Fig. 6).

Selected bond distances and angles for **(1)** are listed in Table 4. The metal–oxygen bond distances in the MnO_6 octahedra have a mean value of 2.20(6) Å. The *cis* and *trans* O–Mn–O bond angles range from 68.5(5)° to 99.0(6)° and from 164.0(4)° to 172.6(7)°, respectively. The distortion of the MnO_6 octahedra, from an octahedron ($\Delta = 0$) to a trigonal prism ($\Delta = 1$) has been quantified by using the Muetterties and Guggenberger method [25]. The value obtained is 6.5%. These results indicate a distortion from the ideal octahedral geometry. The mean value of the selenium–oxygen bond lengths is 1.70(5) Å. The bond valence analysis has been carried out by I.D. Brown calculation method [26] using the $S = \exp[(d/d_0)/B]$ expression, included in the Rietveld program as the subroutine BONDSTR [24], where $d_0 = 1.811$ and 1.790 for Se^{4+} and Mn^{2+} cations, respectively, being $B = 0.370$ for both cations. The calculated oxidation states have values of 3.8(1) and 1.9(1) v.u., for Se^{4+} and Mn^{2+} cations, respectively, in good agreement with those obtained from the structural resolution.

Selected bond distances and angles for **(2)** are listed in Table 4. The mean value for metal–oxygen bond distances in the MnO_6 octahedra is 2.3(1). The *cis* O–Mn–O angles range from 65(2) to 108(2)°, and the *trans* O–Mn–O angles from 154(2) to 175(2)°. The distortion of the MnO_6 octahedra from the ideal octahedral geometry is 2.4% [25]. The mean value of the selenium–oxygen bond distances is 1.6(1) Å. This value is smaller than that found for polymorph **(1)** [1.70(6) Å] and for the $Co(SeO_3) \cdot H_2O$ isotypic phase [1.70(3) Å], probably due to the use of powder data in the Rietveld refinement of the crystal structure of compound **(2)**. The bond valence study [24,26] for Se^{4+} and Mn^{2+} cations of the polymorph **(2)** gives values of 4.1(1) and 1.9(1) v.u., respectively.

3.2. Infrared, UV–Vis and luminescence spectroscopies

The infrared spectra for compounds **(1)** and **(2)** show bands corresponding to the water molecule and the $(SeO_3)^{2-}$ oxoanions. The ν(OH) stretching modes of the

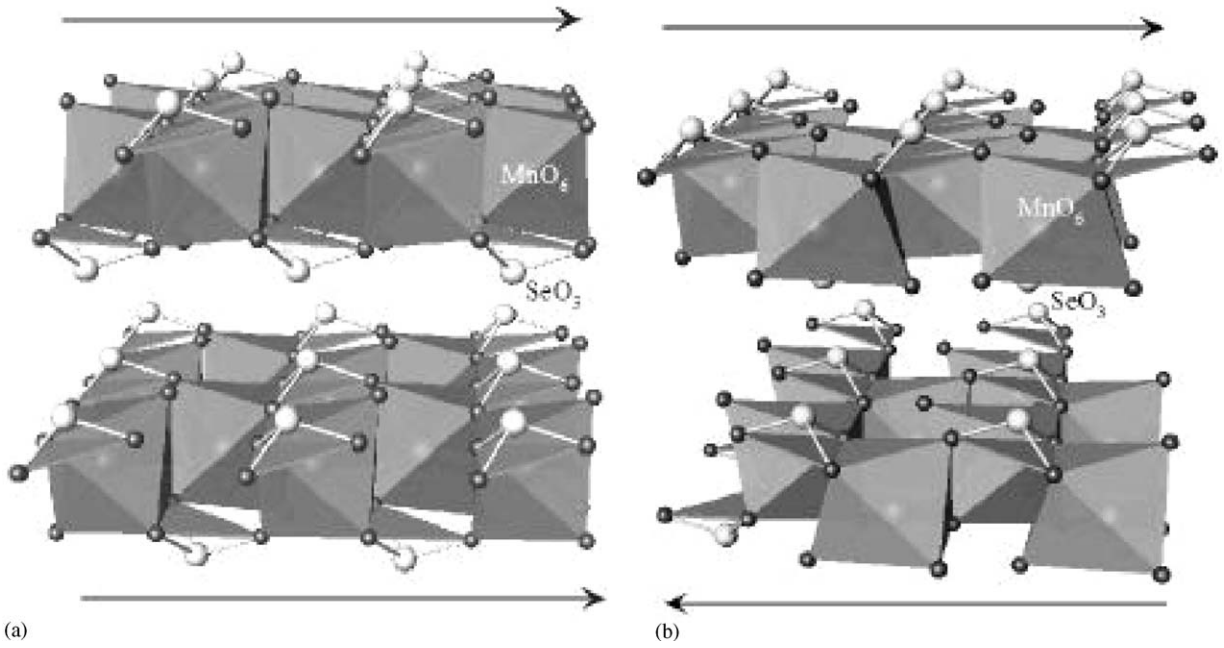

Fig. 3. Layers of the polymorphs (a) **(1)** and (b) **(2)** showing the crystallographically independent MnO_6 octahedra and the $(SeO_3)^{2-}$ anions.

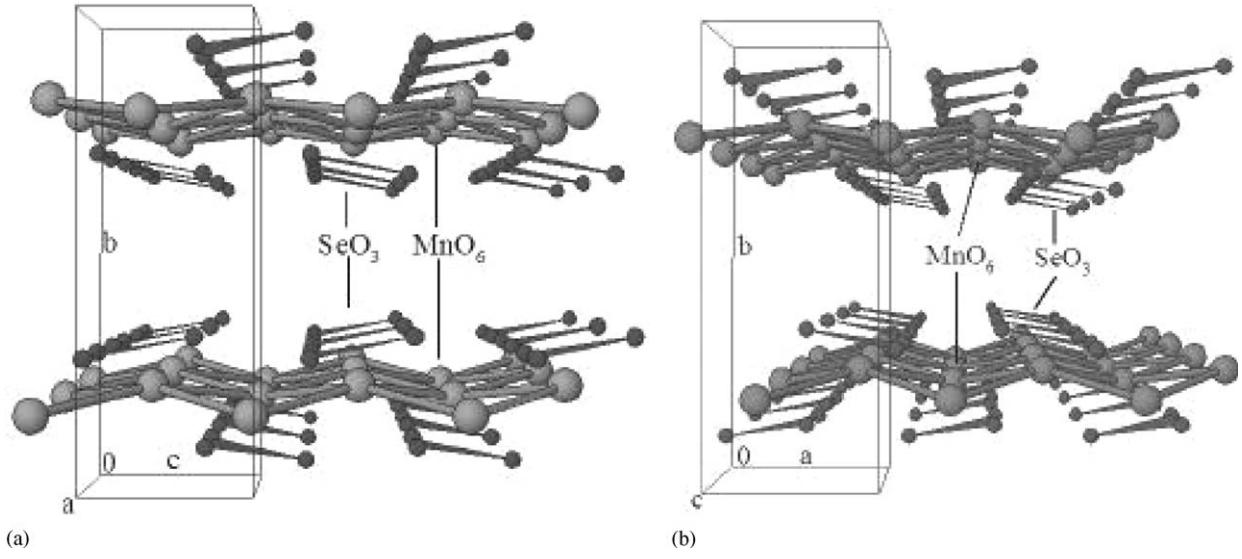

Fig. 4. Arrangement of the layers along the [100] direction for the (a) **(1)** and (b) **(2)**.

water molecules appear in the 3420–2480 and 3415–2860 cm^{-1} ranges and the δ(HOH) deformation at 1625, 1615 cm^{-1} for phases **(1)** and **(2)**, respectively. The symmetric and antisymmetric stretching vibrations, $\nu_s(SeO_3)$, $\nu_{as}(SeO_3)$ and the deformation, $\delta(SeO_3)$, appear at the following frequencies: $\nu_s = 1025$, 995, $\nu_{as} = 850-675$, 850–680 and $\delta = 445\,cm^{-1}$ for compounds **(1)** and **(2)**. The positions observed for these vibrational modes are in good agreement with those expected for these compounds and are similar to those found in the literature for other selenite phases [27–29].

Luminescence measurements of the Mn(II) ions in polymorphs (**1**) and (**2**) have been carried out at 6 K. The emission spectra for both phases obtained under a 420 nm excitation exhibit a unique red emission peaking at 670 and 665 nm for **(1)** and **(2)**, respectively. This emission is characteristic of octahedrally coordinated Mn(II) (d^5) (Fig. 7a). The excitation spectra obtained with emission of 630 nm reveal the spectral distribution of bands corresponding to the excited levels of Mn(II) in octahedral sites (Fig. 7b) [30]. The diffuse reflectance spectra, recordered at room temperature, exhibit several very weak

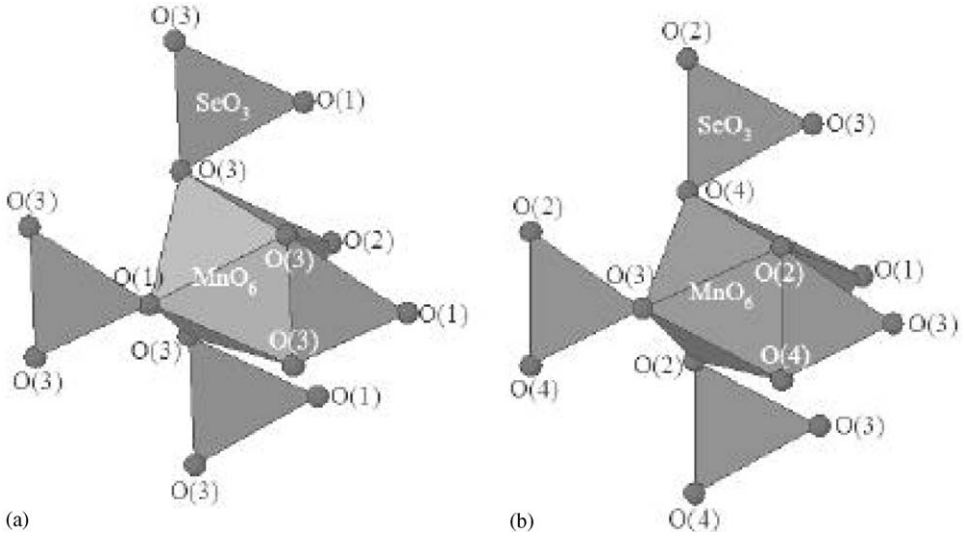

Fig. 5. Coordination environment for the MnO_6 octahedra and the $(SeO_3)^{2-}$ anions in polymorph (a) **(1)** and (b) **(2)**.

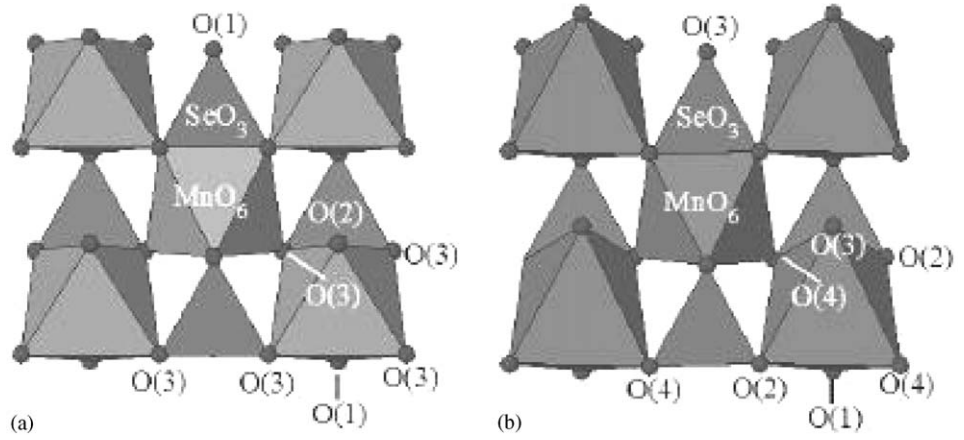

Fig. 6. Link between coordination polyhedra for (a) **(1)** and (b) **(2)**.

spin-forbidden *d–d* bands consistent with Mn^{2+} high spin ions in octahedral geometry. The values are similar to those obtained from the excitation luminescent spectra. Table 5 shows the positions of the bands together with the assignment of the electronic transitions obtained from the luminescence and diffuse reflectance measurements for polymorphs (**1**) and (**2**). Taking into account the results of the luminescence and diffuse reflectance spectroscopies, the *Dq* and Racah parameters have been calculated by fitting the experimental distribution of spectral bands to an energy level diagram for high spin octahedral d^5 system. The *Dq* and Racah parameters are $Dq = 705$, $B = 750$, $C = 3325\,cm^{-1}$ for (**1**) and $Dq = 720$, $B = 745$, $C = 3350\,cm^{-1}$ for (**2**). These results are similar to those found in other octahedrically coordinated Mn^{2+} compounds [9,10]. The *B* values for both selenites are approximately 78% of the value for the free Mn^{2+} cation ($960\,cm^{-1}$), indicating a significant degree of covalence in the Mn–O bonds.

3.3. ESR and magnetic properties

The ESR spectra of phases (**1**) and (**2**) were performed at the X-band on a powdered sample from room temperature to 4.2 K. The spectra of both compounds exhibit isotropic signals due to the presence of magnetically coupled high spin Mn(II) cations (Fig. 8). The signals remain practically unchanged down to 100 and 70 K for **(1)** and **(2)**, respectively; below these temperatures the signals broaden and lose intensity. The ESR signals were fitted by a Lorentzian curve and the "*g*" gyromagnetic factor was calculated for both selenites. The result obtained for both phases was 1.99(1). The thermal evolution of the intensity of the signals shows a continuous increase with cooling the

Table 4
Selected bond lengths (Å) and angles (deg.) for **(1)** and **(2)**

(1)		**(2)**	
Bond distances (Å)			
Se(1)O$_3$ trigonal pyramid			
Se(1)–O(3)^{i}	1.74(1)	Se(1)–O(4)	1.55(8)
Se(1)–O(3)	1.74(1)	Se(1)–O(3)	1.61(5)
Se(1)–O(1)	1.63(1)	Se(1)–O(2)	1.64(5)
Mn(1)O^{6} octahedron			
Mn(1)–O(3)^{ii}	2.28(1)	Mn(1)–O(4)^{ii}	2.29(8)
Mn(1)–O(3)^{v}	2.28(1)	Mn(1)–O(3)^{i}	2.26(5)
Mn(1)–O(3)^{iv}	2.14(1)	Mn(1)–O(3)^{iii}	2.11(5)
Mn(1)–O(3)^{iii}	2.14(1)	Mn(1)–O(2)^{iii}	2.49(5)
Mn(1)–O(2)w	2.21(2)	Mn(1)–O(2)	2.28(5)
Mn(1)–O(1)	2.13(2)	Mn(1)–O(1)w	2.25(7)
Bond angles (deg.)			
Se(1)O$_3$ trigonal pyramid			
O(1)–Se(1)–O(3)^{i}	104.2(5)	O(4)–Se(1)–O(2)	121(3)
O(3)–Se(1)–O(3)^{i}	95.1(7)	O(4)–Se(1)–O(3)	92(3)
O(3)–Se(1)–O(1)	104.2(5)	O(3)–Se(1)–O(2)	99(2)
Mn(1)O$_6$ octahedron			
O(3)^{ii}–Mn(1)–O(1)	82.5(5)	O(4)^{ii}–Mn(1)–O(1)	175(2)
O(3)^{ii}–Mn(1)–O(2)	91.4(5)	O(4)^{ii}–Mn(1)–O(2)	89(2)
O(3)^{ii}–Mn(1)–O(3)^{iii}	164.0(4)	O(4)^{ii}–Mn(1)–O(2)^{iii}	83(2)
O(3)^{ii}–Mn(1)–O(3)^{iv}	96.0(2)	O(4)^{ii}–Mn(1)–O(3)^{iii}	86(2)
O(3)^{ii}–Mn(1)–O(3)^{v}	68.5(5)	O(4)^{ii}–Mn(1)–O(3)^{i}	93(2)
O(3)^{v}–Mn(1)–O(1)	82.5(5)	O(3)^{i}–Mn(1)–O(1)	91(2)
O(3)^{v}–Mn(1)–O(2)	91.8(3)	O(3)^{i}–Mn(1)–O(2)	98.1(2)
O(3)^{v}–Mn(1)–O(3)^{iii}	96.0(2)	O(3)^{i}–Mn(1)–O(2)^{iii}	108(2)
O(3)^{v}–Mn(1)–O(3)^{iv}	164.1(3)	O(3)^{i}–Mn(1)–O(3)^{iii}	154(2)
O(3)^{iv}–Mn(1)–O(1)	91.4(5)	O(3)^{iii}–Mn(1)–O(1)	92(2)
O(3)^{iv}–Mn(1)–O(2)	93.3(4)	O(3)^{iii}–Mn(1)–O(2)	89(2)
O(3)^{iv}–Mn(1)–O(3)^{iii}	99.0(6)	O(3)^{iii}–Mn(1)–O(2)^{iii}	65(2)
O(3)^{iii}–Mn(1)–O(1)	91.5(4)	O(2)^{iii}–Mn(1)–O(1)	87(2)
O(3)^{iii}–Mn(1)–O(2)	93.3(4)	O(2)^{iii}–Mn(1)–O(2)	170(2)
O(2)w–Mn(1)–O(1)	172.6(7)	O(2)–Mn(1)–O(1)	101(2)

Symmetry codes used to generate the equivalent atoms for **(1)** and **(2)**.
(1) i $= -x+\frac{3}{2}, y, z$; ii $= x, y, z-1$; iii $= x+\frac{1}{2}, -y+\frac{1}{2}, z+\frac{1}{2}$, iv $= -x+1, -y+\frac{1}{2}, z+\frac{1}{2}$; v $= -x+\frac{3}{2}, y, z+1$.
(2) i $= x, y, 1+z$, ii $= -\frac{1}{2}+x, \frac{1}{2}-y, \frac{1}{2}+z$; iii $= \frac{1}{2}+x, \frac{1}{2}-y, \frac{1}{2}+z$.

sample up to 25 and 30 K, for compounds (**1**) and (**2**), respectively. Finally, a dramatic decrease of the intensity occurs (Fig. 9). These results suggest the existence of antiferromagnetic interactions in both polymorphs. The temperature dependence of the line width shows a weak increase from room temperature to 100 K. Below this temperature the line width increases vigorously down to 4.2 K, probably due to a strong spin correlation [31].

Magnetic measurements for polymorphs (**1**) and (**2**) were performed on powdered samples at 1000 G from room temperature to 5 K, in the modes Zero Field Cooling (ZFC) and Field Cooling (FC) modes, being similar the results obtained for both cases (Figs. 10a and b). The molar magnetic susceptibility of both phases, χ_m, increases with decreasing temperature and reaches a maximum at 14 and 17 K for **(1)** and **(2)**, respectively, indicating the establishment of a magnetic ordering. Below these temperatures the magnetic susceptibility decreases continuously up to 5 K. The form of these maxima with an appreciable width suggests the existence of magnetic couplings of low dimensionality. The thermal evolution of the molar magnetic susceptibility follows the Curie–Weiss law in the 40–300 K and 45–300 K ranges, for **(1)** and **(2)**, respectively. The values of the Curie and Curie–Weiss constant are 4.50 cm^3K/mol and −50.0 K for **(1)** and **(2)**, in good agreement with the existence of one Mn(II) cation in the unit formula of these compounds. The $\chi_m T$ vs. T curve decreases continuously from 3.80 and 3.85 cm^3K/mol at room temperature up to 0.25 and 0.18 cm^3K/mol at 5 K, for the polymorphs **(1)** and **(2)**, respectively.

Taking into account the structural features of these polymorphs which show the existence of sheets separated by, approximately, 3.3 Å, a three-dimensional magnetic model can be disregarded for the analysis of the magnetic behavior. At first glance, from the magnetic point of view the layers inside could be considered, simultaneously, the existence of triangular and square planar antiferromagnetic lattices (see Fig. 11a and b).

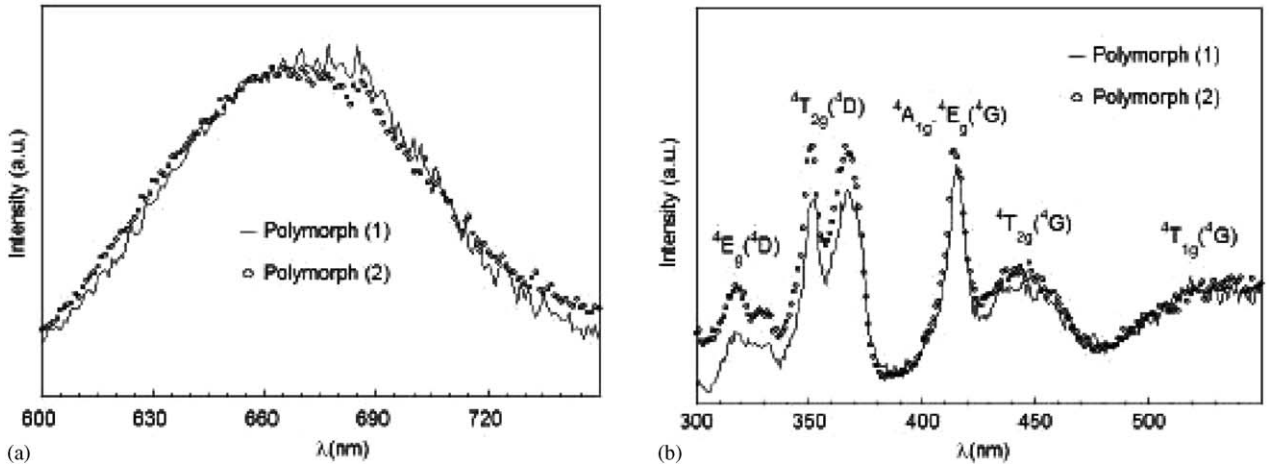

Fig. 7. (a) Luminescent emission spectra for phases **(1)** and **(2)** and (b) luminescent excitation spectra for phases **(1)** and **(2)**.

Table 5
Assignment of the electronic transitions obtained from the luminescence and diffuse reflectance measurements for **(1)** and **(2)**

Assignment v (cm^{-1})	$Mn(SeO_3)\cdot H_2O$ **(1)**		$Mn(SeO_3)\cdot 2H_2O$ **(2)**	
	Luminescence	Diffuse reflectance	Luminescence	Diffuse reflectance
$^6A_{1g}(^6S)\rightarrow{}^4T_{1g}(^4G)$	18345	18350	18350	18350
$^6A_{1g}(^6S)\rightarrow{}^4T_{2g}(^4G)$	22475	22470	22575	22570
$^6A_{1g}(^6S)\rightarrow{}^4A_{1g}(^4G);\ {}^4E_g(^4G)$	24100	24095	24220	24215
$^6A_{1g}(^6S)\rightarrow{}^4T_{2g}(^4D)$	27785	27780	28565	28570
$^6A_{1g}(^6S)\rightarrow{}^4E_g(^4D)$	30770	30770	31540	31545

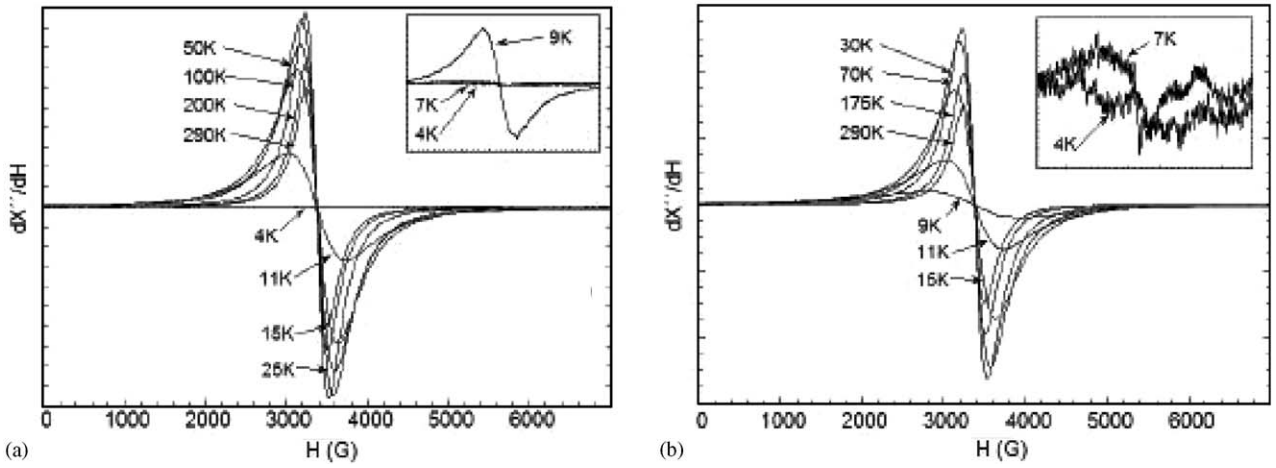

Fig. 8. Thermal variation of the ESR spectra for (a) **(1)** and (b) **(2)**.

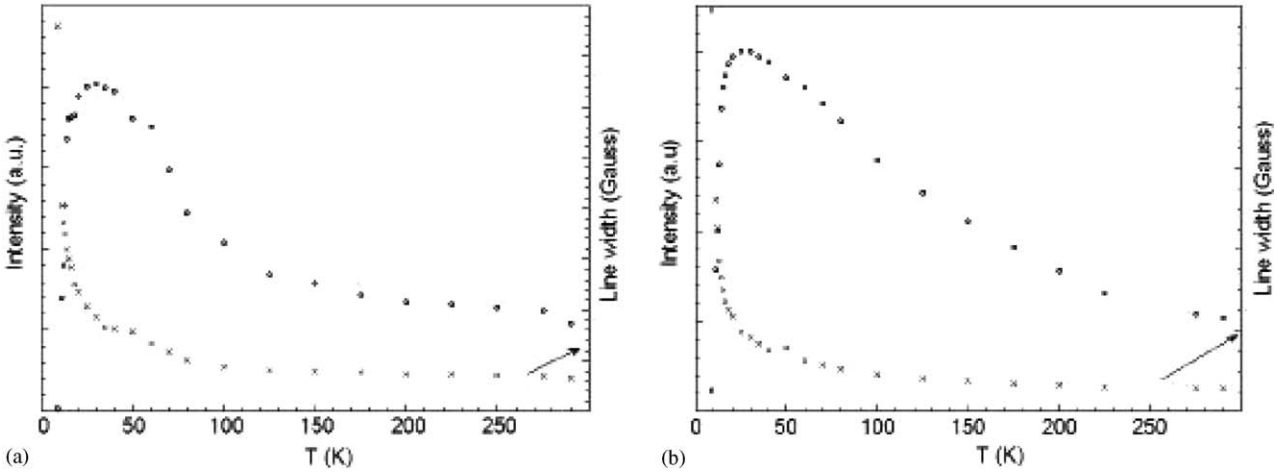

Fig. 9. Thermal variation of the intensity and line width for (a) **(1)** and (b) **(2)**.

Considering this situation, the experimental magnetic data were fitted to the expressions derived by Rushbrooke and Wood for the triangular (Eq. (1)) and square-planar (Eq. (2)) lattices [32]:

$$\chi_m = (35Ng^2\beta^2/12kT) \times[1 + 35x + 221.667x^2 - 1909.83x^3 + 6156.92x^4 + 84395.9x^5 - 1522000x^6]^{-1}, \quad (1)$$

$$\chi_m = (35Ng^2\beta^2/12kT)[1 + 23.33x + 147.78x^2 - 405.48x^3 + 8171.3x^4 + 64961.8x^5 - 158110x^6]^{-1}, \quad (2)$$

where, $x = |J|/kT$, k is the Boltzman constant, N the Avogadro's number and β the Bohr magneton. The solid lines in Fig. 10 show the best fits obtained. These results indicate a disaccord between the experimental and theoretical data when the triangular lattice model is considered. However, the fit is reasonably good when the square-planar

model is used, with the magnetic exchange parameters, $J/k = -0.83$, -0.91 K and $J'/k = -0.97$, -1.20 K, for the polymorphs **(1)** and **(2)**, respectively. The "g" value was 1.99, obtained from the ESR measurements.

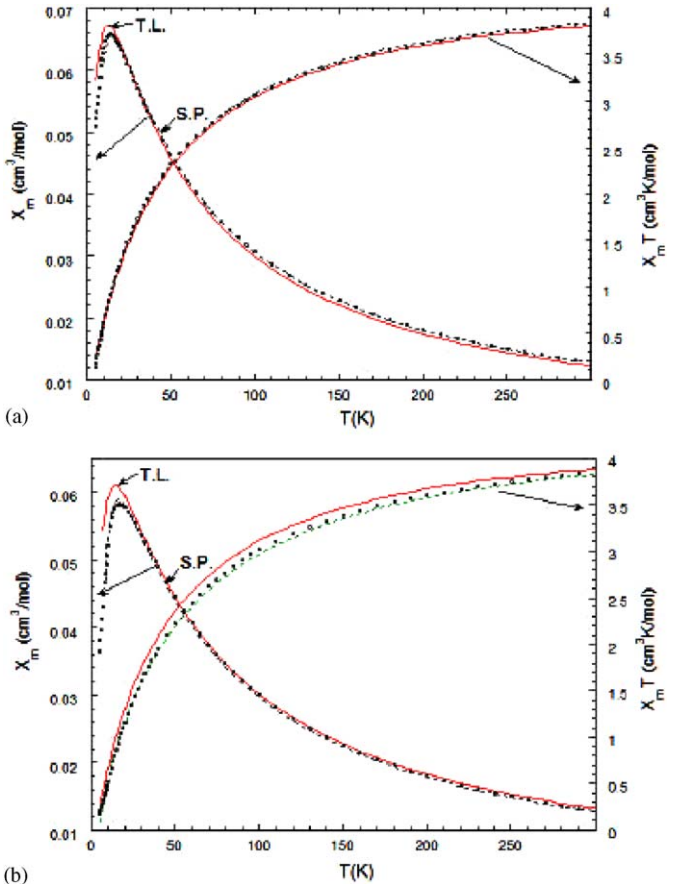

Fig. 10. Thermal variation of the χ_m and $\chi_m T$ curves for (a) **(1)** and (b) **(2)**. The solid lines shown the best fit for the models triangular-planar (TP) and square-planar (SP) lattices.

It is necessary to indicate that in order to obtain a good fit, a high value of the J'/k parameter, on the basis of the approximation of the molecular field [33], is necessary to consider additionally to the J-exchange parameter associated to the Rushbrooke and Wood equation. This parameter could explain the contribution of the triangular lattice to the total magnetic exchange in these phases. Consequently, these results suggest that the theoretical proposed model must be considered with caution.

4. Concluding remarks

Two new polymorphs with formula $Mn(SeO_3)\cdot H_2O$ have been synthesized and their crystal structures resolved from single-crystal and powder diffraction data. The phases have been characterized by chemical analysis, thermal and IR measurements. The diffuse reflectance and luminescence studies indicate slightly distorted octahedral geometry for the Mn(II) cations. The magnetic analysis shows similar antiferromagnetic couplings in both phases. The J-exchange parameters have been calculated by fitting the experimental data with a model for a square-planar lattice.

Acknowledgments

This work has been financially supported by the "Ministerio de Educación y Ciencia" (MAT-2004-02071) and the "Universidad del País Vasco" (UPV/EHU) (9/UPV00130.310-15967/2004; 9/UPV00169.310-13494/2001). The authors thank the technicians of SGIker, Dr. J.P. Chapman and Dr. I. Orue, financed by the "National Program for the Promotion of Human Resources within the National Plan of Scientific Research, Development and Innovation"—"Ministerio de Ciencia y Tecnología" and "Fondo Social Europeo (FSE)", for the X-ray diffraction and magnetic measurements, respectively.

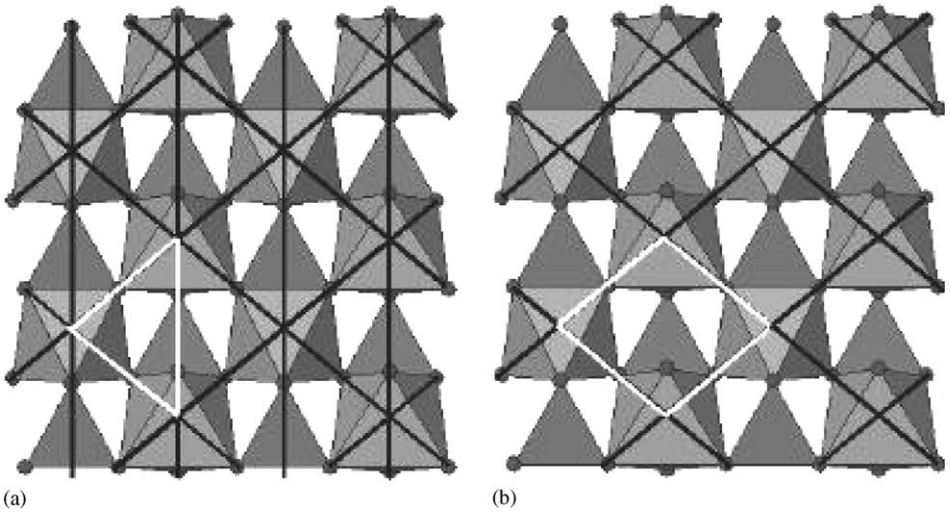

Fig. 11. Schematic representation of (a) the triangular-planar and (b) the square-planar lattices.

Dr. A. Larrañaga wishes to thank the Gobierno Vasco/Eusko Jaurlaritza for funding.

References

[1] S.M. Kauzlarich, P.K. Dorhout, J.M. Honig, J. Solid State Chem. 149 (2000) 3.

[2] C.N.R. Rao, J. Gopalakrihnan, New Directions in Solid State Chemistry. Structure, Synthesis, Properties, Reactivity and Materials Design, Cambridge University Press, Cambridge, 1986.

[3] M. Koskenlinna, Structural Features of Selenium(IV) Oxoanion Compounds, Jouko Koskikallio, Finland, 1996.

[4] K. Byrappa, M. Yoshimura, Handbook of Hydrothermal Technology, Hard Cover, 2001.

[5] (a) B. Engelen, K. Boldt, K. Unterderweide, U. Baumer, Z. Anorg. Allg. Chem. 621 (1995) 331;
(b) M. Koskenlinna, J. Kansikas, T. Leskela, Acta Chem. Scand. 48 (1994) 783;
(c) Z. Micka, I. Nemec, P. Vojtisek, J. Ondracek, J. Holsa, J. Solid State Chem. 112 (1994) 237;
(d) J. Valkonen, M. Koskenlinna, Acta Chem. Scand., Ser. A 32 (1978) 603;
(e) W.T.A. Harrison, G.D. Stucky, A.K. Cheetham, Eur. J. Solid State Inorg. Chem. 32 (1993) 347.

[6] (a) M. Wildner, Monatsh. Chem. 122 (1991) 585;
(b) V.P. McManus, W.T.A. Harrison, A.K. Cheetham, J. Solid State Chem. 92 (1991) 253;
(c) H. Efenberger, J. Solid State Chem. 70 (1987) 303;
(d) W.T.A. Harrison, G.D. Stucky, R.E. Morris, A.K. Cheetham, Acta Crystallogr., Sect. C 48 (1992) 1365;
(e) X. Dongrong, H. Yu, W. Enbo, A. Haiyan, L. Jian, L. Yangguang, X. Lin, H. Changwen, J. Solid State Chem. 177 (2004) 2706.

[7] (a) M. Koskenlinna, L. Niinisto, J. Valkonen, Acta Chem. Scand., Ser. A 30 (1976) 836;
(b) G. Meunier, M. Bertaud, Acta Crystallogr., Sect. B 30 (1974) 2840;
(c) F.C. Hawthorne, L.A. Groat, T.S. Ercit, Acta Crystallogr., Sect. C 43 (1987) 2042;
(d) W.T.A. Harrison, A.V.P. McManus, A.K. Cheetham, Acta Crystallogr., Sect. C 48 (1992) 412.

[8] K. Kohn, I. Katsuhiko, O. Horie, S.I. Akimoto, J. Solid State Chem. 18 (1976) 127.

[9] A. Larrañaga, J.L. Mesa, L. Lezama, J.L. Pizarro, R. Olazcuaga, M.I. Arriortua, T. Rojo, J. Chem. Soc., Dalton Trans. (2002) 3447.

[10] A. Larrañaga, J.L. Mesa, J.L. Pizarro, L. Lezama, J.P. Chapman, M.I. Arriortua, T. Rojo, J. Chem. Soc., Dalton Trans. (2005) 1727.

[11] W.T.A. Harrison, M.L.F. Philips, J. Stanchfield, T.M. Nenoff, Angew. Chem., Int. Ed. 39 (2000) 3808.

[12] A. Choudhury, D. Udayakumar, C.N.R. Rao, Angew. Chem., Int. Ed. 41 (2002) 158.

[13] D. Udayakumar, C.N.R. Rao, J. Mater. Chem. 13 (2003) 1635.

[14] Powder Diffraction File Inorganic and Organic, File 78-390, Pennsylvania, 1995.

[15] CRYSALIS Version 1.70: Program for the Data Reduction. Oxford Diffraction Ltd., Oxford, England.

[16] G.M. Sheldrick, SHELXS 97: Program for the Solution of Crystal Structures, University of Göttingen, Göttingen, Germany, 1997.

[17] L.J. Farrugia, J. Appl. Crystallogr. 32 (1999) 837.

[18] G.M. Sheldrick, SHELXL 97: Program for the Refinement of Crystal Structures, University of Göttingen, Göttingen, Germany, 1997.

[19] International Tables for X-ray Crystallography, vol. IV, Kynoch Press, Birmingham, England, p. 99.

[20] B. Engelen, H. Mueller, Z. Kristallogr. 213 (5) (1998) 275.

[21] T. Roisnel, J. Rodriguez Carvajal, WinPLOTR, A Graphical Tool for Powder Diffraction, 2001.

[22] (a) P.E. Werner, TREOR, Trial and Error Program for Indexing of Unknown Powder Patterns, 1984;
(b) P.E. Werner, J. Appl. Crystallogr. 18 (1985) 367.

[23] E. Dowty, ATOMS, A Computer Program for Displaying Atomic Structures, Shape Software, 521 Hidden Valley Road, Kingsport, TN, 1993.

[24] J. Rodriguez Carvajal, FULLPROF Program, Rietveld Pattern Matching Analysis of Powder Patterns, 1994.

[25] E.L. Muetterties, L.J. Guggenberger, J. Am. Chem. Soc. 96 (1974) 1748.

[26] I.D. Brown, D. Altermatt, Acta Cryst. B 41 (1985) 244.

[27] K. Nakamoto, Infrared Spectra of Inorganic and Coordination Compounds, Wiley, New York, 1986.

[28] V.P. Verma, Thermochim. Acta 327 (1999) 63.

[29] A.S. Povarennykh, L.A. Onishchenko, Geol. Zh. 33 (6) (1973) 98.

[30] (a) T.Y. Sugano, J. Phys. Soc. Jpn. 9 (1954) 753;
(b) A.B.P. Lever, Inorganic Electronic Spectroscopy, Elsevier Science, Amsterdam, Netherlands, 1984.

[31] (a) H.W. Wijn, L.R. Walker, J.L. Daris, H. Guggenheim, J. Solid State Chem. Commun. 11 (1972) 803;
(b) P.M. Richards, M.B. Salamon, Phys. Rev. B 9 (1975) 32;
(c) A. Escuer, R. Vicente, M.A.S. Goher, F. Mautner, Inorg. Chem. 34 (1995) 5707;
(d) A. Bencini, D. Gatteschi, EPR of Exchange Coupled Systems, Springer, Berlin, 1990;
(e) T.T.P. Cheung, Z.G. Soos, R.E. Dietz, F.R. Merrit, Phys Rev. B 17 (1978) 1266.

[32] G.S. Rushbrooke, P.S. Wood, Mol. Phys. 1 (1958) 257.

[33] R.L. Carlin, Magnetochemistry, Springer, Berlin, Heidelberg, 1986.